Hindawi Publishing Corporation
Advances in Condensed Matter Physics
Volume 2015, Article ID 729186, 8 pages
http://dx.doi.org/10.1155/2015/729186

Research Article

Rebirth of Liquid Crystals for Sensoric Applications: Environmental and Gas Sensors

P. V. Shibaev,[1] M. Wenzlick,[1] J. Murray,[1] A. Tantillo,[1] and J. Howard-Jennings[2]

[1]*Department of Physics, Fordham University, 441 East Fordham Road, New York, NY 10458, USA*
[2]*The Bronx High School of Science, 75 West 205th Street, New York, NY 10468, USA*

Correspondence should be addressed to P. V. Shibaev; shibayev@fordham.edu

Received 15 December 2014; Revised 23 February 2015; Accepted 5 March 2015

Academic Editor: Victor V. Moshchalkov

Films and droplets of liquid crystals may soon become an essential part of sensitive environmental sensors and detectors of volatile organic compounds (VOCs) in the air. In this paper a short overview of recent progress in the area of sensors based on liquid crystals is presented, along with the studies of low molar mass liquid crystals as gas sensors. The detection of VOCs in the air may rely on each of the following effects sequentially observed one after the other: (i) slight changes in orientation and order parameter of liquid crystal, (ii) formation of bubbles on the top of the liquid crystalline droplet, and (iii) complete isotropisation of the liquid crystal. These three stages can be easily monitored by a photo camera and/or optical microscopy. Detection limits corresponding to the first stage are typically lower by a factor of at least 3–6 than detection limits corresponding to isotropisation. The qualitative model taking into account the reorientation of liquid crystals is presented to account for the observed changes.

1. Introduction

Liquid crystals discovered in the nineteenth century by Reinitzer and studied by Lehman [1, 2] were subsequently almost forgotten in the beginning of the twentieth century, at last experiencing a rebirth in the middle of the last century since they became a principal material used for visualization of information in a variety of devices that rapidly filled our everyday life. The production of displays and indicators increased by orders of magnitude since the 1970s due to a rapidly developing market that was not only a major driving force for designing novel commercial liquid crystalline compositions, but also a generous supporter of developing the fundamental science of liquid crystals [3]. By the end of the twentieth century the major theoretical models describing the behavior of liquid crystals were already created and tested, and the market was already filled with the displays and indicators with substantially improved resolution and color characteristics. One decade later the resolution of displays has increased so dramatically that the human eye is not able to really see and appreciate any further improvement. The switching time of liquid crystals has also decreased significantly allowing watching high resolution videos and producing stereo images. Of course, there is still room for further progress in display technology, for example, development of flexible displays and 3D displays.

At the same time, the very nature of liquid crystals, namely, the anisotropy of molecular shape and, therefore, optical anisotropy, makes them very attractive for other areas of industrial applications, including the area of chemical sensors. Indeed, the changes in the orientation of liquid crystals due to minor changes in surface energy or in the chemical environment can be easily detected by a variety of optical methods. Moreover, the structure of liquid crystalline matrices can also be modified and tuned in order to make them more sensitive to specific environmental agents [4]. In this paper we discuss recent progress of using liquid crystals as sensors of environmental agents, concentrating on gas sensors, and also present the results of the research conducted on nematic and chiral liquid crystals employed as detectors of volatile organic compounds (VOCs) in the air.

2. Liquid Crystals as Environmental Sensors

Recently, research on detection of biological and chemical agents by means of liquid crystals [4–9] has progressed in

the areas of all major types (nematic, smectic, and cholesteric) of liquid [5, 8] and polymer [4, 6, 7] liquid crystalline materials. In case of nematic and smectic LC materials one of the major indicators of environmental agents presence was a textural change in the visual appearance of liquid crystals [5, 8]. Much effort was dedicated to solving the problem of the detection of biological molecules in aqueous media by analyzing morphological changes in free standing low molar mass liquid crystalline films and droplets [5] or films deposited on functionalized surfaces [8]. Liquid crystalline polymers and polymer networks were also explored for detection of organic solvents, pH changes in water, and amino acids [4, 6, 7]. Proton sensitive glucose sensors employing classical 4-cyano-4-pentylbiphenyl (5CB) material were successfully tested in [8]. The short overview of using LCs for environmental detection is given in [9].

One of the first attempts to use LCs as detectors of volatile organic compounds (VOCs) is described in [10]. In this work a nematic-isotropic transition was used as an indicator of VOC exposure; the absorption of VOC molecules from the air first led to the lower isotropisation temperature and then to a transition to isotropic state. It was determined that one of the most sensitive compounds in a class of nematic LCs was MBBA (4-methoxybenzylidene-4-butylaniline) or its mixtures with other derivatives of butylaniline. In [11], the discotic liquid crystals based on phthalocyanines were used to detect low concentration of nitrogen oxide. Functionalized cholesterol derivatives forming cholesteric films with a selective reflection band in a visible part of the spectrum were studied in [12] as promising sensors for detecting amine vapors. The absorption of VOCs resulted in a spectral shift of the selective reflection band position. The use of cholesteric liquid crystals for monitoring gas concentration was also considered in [13], where reactive chiral dopants changed helical twisting power and, therefore, the position of the selective reflection band, as well as the sample color, by reacting with carbon dioxide. Cholesteric liquid crystals with the selective reflection band changing its position when material was exposed to gases were further explored in [14] for sensing such volatile compounds as methanol, ethanol, tetrahydrofuran, and so forth. The liquid crystal was shown to be the most responsive to polar solvents; the sensitivity threshold for ethanol was determined to be ca. 0.5% of solvent in the air. Aldehyde vapors were detected by cholesteric liquid crystals doped with dodecylamine in [15]. The major mechanism of detection was based on a chemical reaction between amine and aldehyde groups. The similar principle (i.e., the reaction between butylamine and lauric aldehyde) was recently employed in [16] for a nematic film changing its orientation during the reaction. Mixtures of carbon nanotubes with chiral cyanobiphenyl derivatives were recently studied in [17, 18] as promising VOC detectors: The prototype for estimation of acetone vapor concentration in the range 250–550 ppm was built and tested. Carbon nanotubes were also used in sensors based on polymer dispersed liquid crystals; these sensors may become an interesting alternative to sensors based on pure liquid crystals [19]. The nanotechnology platform based on liquid crystals and targeted to detection of biological threads and toxic gases is discussed in [20].

3. Liquid Crystals as Sensors of Volatile Organic Compounds

Here we describe the principles that can be used for detection of low concentrations of VOC in the air. We are mostly focused on a study of optical response of common low molar mass liquid crystals to different volatile organic compounds (VOCs) before LCs experience the transition to isotropic state. The focus on the developing changes in interference pattern (under gas absorption) in nematic droplets instead of focusing on transition to isotropic state and/or textural changes allowed us to decrease the detection limit of different VOCs by a factor of 3–6 depending on the chemical structure of particular VOC.

A controlled gas atmosphere was created inside a sealed Petri dish (container) that was placed on a microscope table. Liquid crystal sample (a droplet with a diameter ca. 50–150 microns) was placed inside the container and a few microliters of VOC liquid were injected onto the bottom of the container through a small hole made in the upper plate. The hole was sealed by aluminum tape immediately after the injection. The rapid evaporation and a uniform gas atmosphere inside the container were facilitated by the installation of a small fan. Tin dioxide gas sensors (MQ-3 and MQ-303 from Hanwei Electronics) were also installed inside the container. The sample was illuminated from the bottom and all observations and optical measurements were performed through the microscope. The photos were taken by a photo camera (Samsung MV800 with CMOS sensor) attached to the microscope. Different types of nematic liquid crystals were used in experiments (MBBA, pentyl-cyanobiphenyl, and mixtures of these nematic LCs with chiral perillyl alcohol and ethylbenzylamine). All chemicals were purchased from Sigma-Aldrich and used as received. Nematic and chiral droplets were put on microscope slides covered either with polyimide layers promoting planar orientation or with sodium dodecyl sulphate promoting homeotropic orientation of LC molecules and, therefore, a formation of fingerprint structure.

After injection of VOC liquid into the container, its evaporation starts immediately and concentration rapidly rises and reaches saturation at approximately one minute after the injection. The typical concentration dependence on time (that was measured by the tin dioxide sensor) is shown in Figure 1. It takes some time for the gas to diffuse inside the droplet and induce a nematic-isotropic transition at a stage where vapor concentration reaches a maximum (the area "Isot" between the arrows in Figure 1). The isotropisation transition is normally preceded by the formation of multiple bubbles on the top of the droplet (the area marked as "Bubl" between arrows in Figure 1) and intense mass transfer between the volumes of LC saturated with the gas and the rest of the sample. Interestingly, the presence of VOCs in the air can actually be detected even at an earlier stage just by following the changes in the interference pattern formed by

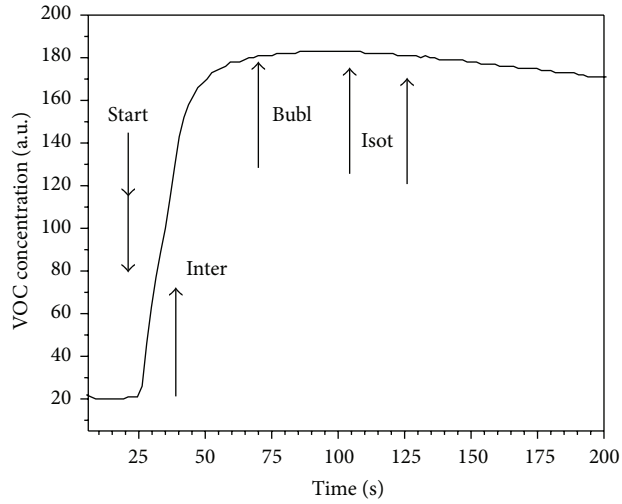

Figure 1: Typical dependence of ethanol concentration in the container as a function of time (measured by tin oxide sensor). Area marked as "Isot" corresponds to isotropisation, area "Bubl" corresponds to bubbles formation, and area "Inter" corresponds to changes in interference pattern. Injection of ethanol occurred at ca. 20th s (this point is marked as "Start").

light passing through the sample. Initial interference pattern is shown in Figure 2(a). The sequence of changes observed in liquid crystalline droplets under increasing concentration of VOCs is shown in Figures 2(a)–2(c). The widening of interference is seen in Figure 2(b). At the second stage the mass transfer starts to be visible (Figure 2(c)), and at the third stage isotropisation occurs (Figure 2(d)). The amount of VOC inducing the transition from the nematic to the isotropic state depends on the chemical composition of LC matrix and the nature of VOC. For ethyl alcohol and MBBA matrix the transition happens at concentrations of about 100 μL/L; for ethyl alcohol and LC matrix based on cyanobiphenyl derivatives the isotropisation occurs at concentrations higher than 250 μL/L. The "bubbling" stage, preceded by subtle changes in interference pattern at the edge of the droplet, is most likely just a manifestation of phase separation between isotropic areas and nematic areas (areas with different order parameter). The detection limits of VOCs can be significantly reduced if these interference pattern variations are analyzed and gas detection is based on the analysis of these variations.

Let us consider what causes the variations in interference pattern. Both the order parameter and the orientation of LC matrix are affected by the VOC diffusion in the thinner part of the droplet, close to its edge (Figure 3). From many observations of the droplets in a gas atmosphere it seems that, at the initial stage of gas diffusion inside the droplet, orientation of the director does not significantly change. This means that gas diffusion results in the formation of an outer diffusion layer on the top of the droplet with lower order parameter. The director profile (predominant orientation of molecular axis) inside nematic droplet is shown in Figure 3 by dashed line: the director is parallel to the substrate and almost perpendicular to droplet's surface, as it often happens in free standing nematic samples. Light rays falling on the droplet from the bottom will experience multiple reflections inside the droplet and may induce the appearance of interference pattern; however, the contrast of the pattern must be rather weak since multiple light reflections from the surfaces inside the droplet have to lead to a decrease of its intensity. Indeed, the reflection coefficient in case of normal incidence is proportional to the ratio $|n_1 - n_{av}|/(n_1 + n_{av})$, where $n_1 = 1.52$ and $n_{av} = 1.65$. This leads to a reflection of 24-25% of light from the surface of LC and air and to a reflection 4-5% of light from the border between LC droplet and glass. Thus, total light intensity contributing to multiple reflection interference is proportional to the product of these two and is only 1% of incoming light intensity. This is too small compared to observed intensities. The observations also confirm that the interference pattern has the highest contrast when it is observed between the crossed polarizers. Moreover, the pattern changes its brightness in accordance with the law $\sin^2(2 * \varphi)$, where φ is the angle between polarizers, which allows ruling out possible contributions from multiple reflections. Thus, the major contribution to interference pattern comes from components of ordinary and extraordinary waves when the electric vector of light forms an angle with the direction of planar orientation on the substrate. It is assumed that the gas diffusion results in the formation of a thin outer layer on a droplet with a lower order parameter S. Changes in order parameter affect both ordinary and extraordinary refractive indexes of the birefringent nematic matrix. This can be described by the following relationship [21]:

$$n_{||} = n_{av} + \frac{2}{3} S\Delta n, \tag{1a}$$

$$n_{\perp} = n_{av} - \frac{1}{3} S\Delta n. \tag{1b}$$

Index $n_{||}$ ($n_{\perp}$) corresponds to a refraction measured along (perpendicular) the direction of ideally oriented planar nematic sample. Thus the diffusion of VOC molecules results in changes of indicatrix ellipsoid (see Figure 3) that becomes less elongated until it adopts a spherical shape at isotropisation stage. The propagation of light inside the droplet was modelled by using the technique of Jones matrices. The expression for light intensity coming out of the droplet placed between two polarizers crossed at an angle φ is given by the following equation [22]:

$$I(x) \sim \frac{I_0}{2} \sin^2(2\varphi) \sin^2\left(\frac{\pi (n_{\text{eff}} - n_{\perp}) d}{\lambda}\right), \tag{2a}$$

where

$$n_{\text{eff}} = n_{\perp}\left(\frac{2}{\pi}\int_0^{\pi/2} \frac{1}{\sqrt{1 - R\sin^2(\theta(y))}}\right), \quad R = \frac{{n_{||}}^2 - {n_{\perp}}^2}{{n_{||}}^2}, \tag{2b}$$

and $\theta(y)$ is the angle that the director makes with substrate (this angle is a function of the position inside the droplet;

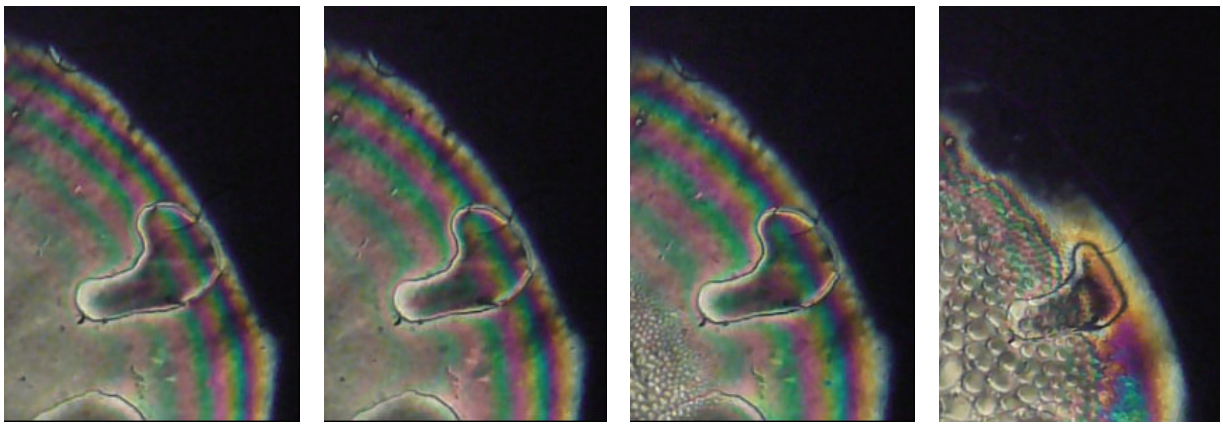

(a) (b) (c) (d)

Figure 2: Typical sequence of changes observed in nematic droplets through crossed polarizers (compared to stages in Figure 1): (a) before injection of VOC, (b) interference pattern change, (c) bubbles formation, and (d) beginning isotropisation.

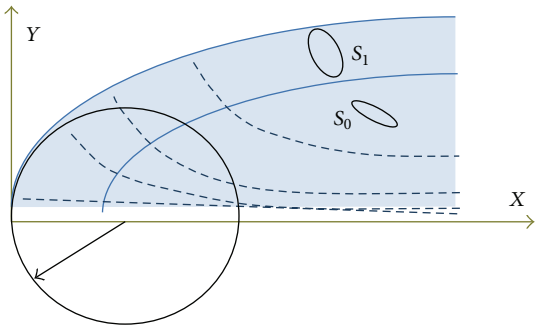

Figure 3: Schematic representation of the droplet in VOCs atmosphere: gas diffusion results in the formation of outer layer with lower order parameter (see also explanations in the text).

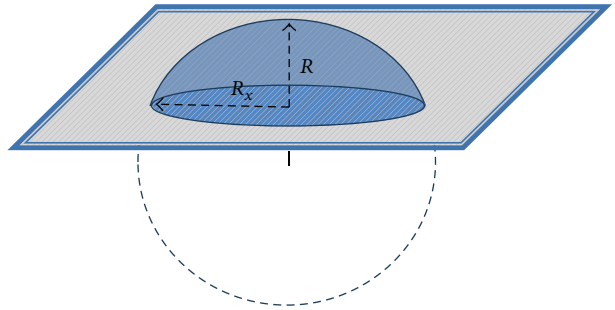

Figure 4: The spherical shape of the droplet used in simulations.

see Figure 3). In spite of the apparent simplicity of (2b) it requires the creation of a mesh inside the droplet with a size much smaller than the wavelength of light and the adoption of (i) a director profile defined by angle $\vartheta(y)$ and (ii) order parameter matrix $S(x, y)$ defined for each mesh node inside the droplet. The refractive indices are calculated from (1a) and (1b). The numerical integration over the droplet's mesh then provides the results for light intensity as a function of distance from the edge of the droplet.

In our model calculations we assumed that the shape of the droplet near its edge can be represented as a sphere. Figure 3 shows the part of the droplet that can be rather satisfactory represented by a spherical surface and Figure 4 shows the droplet's shape used in calculation. The wetting angle can be adjusted by changing the radius of the droplet and its height. As it was mentioned above, the calculations of interference pattern in accordance to (2a) are essentially reduced to calculations of effective refractive index (2b). In our calculations a fine rectangular mesh (with a side 110 nm) was created inside the droplet and the angle that the director forms with the substrate was slowly decreasing from the value corresponding to perpendicular orientation at the top of the droplet to zero at the substrate. The refractive indices of the droplet were assumed to be the same as those for MBBA: $n_{av} = 1.65$ and $\Delta n = 0.3$. The results of the calculations for the droplet of radius 90 microns are shown in Figure 5. The increase of the thickness of the outer layer as diffusion progresses results in the expanding interference pattern that becomes wider with the peaks shifting away from the edge.

The experimental data for MBBA liquid crystal and alcohol vapor confirm the outcome of the model. First, it can be easily seen that the minima of light intensity shift away from the droplet's edge (this becomes visible before the bubbling or isotropisation occurs) even from the photos in Figures 2(a) and 2(b). Second, the plot of light intensity as a function of a distance from the edge also confirms the shift of the pattern (Figure 6). The intensity was determined by the analysis of photos performed with ImageJ software and presented in Figure 6 for different times. The longer time corresponds to wider outer diffusion layer shown in Figure 3. Experimental observations only provide us with time-dependent changes in interference pattern. Our model allows us to translate these data to time dependence of diffusion length, if a diffusion coefficient of a particular VOC into the droplet is known and maximum concentration of VOC inside the matrix is measured. Unfortunately, there are no systematic studies on diffusion coefficients of different

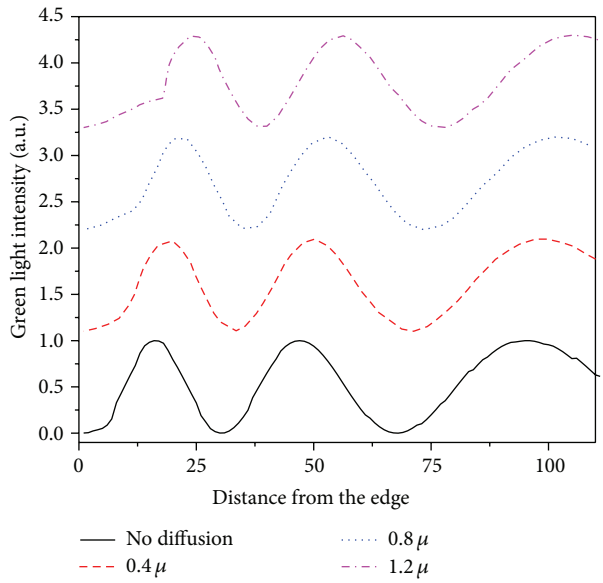

FIGURE 5: Results of light intensity calculations for interference pattern. The formation of the outer layer due to gas diffusion results in widening of the peaks.

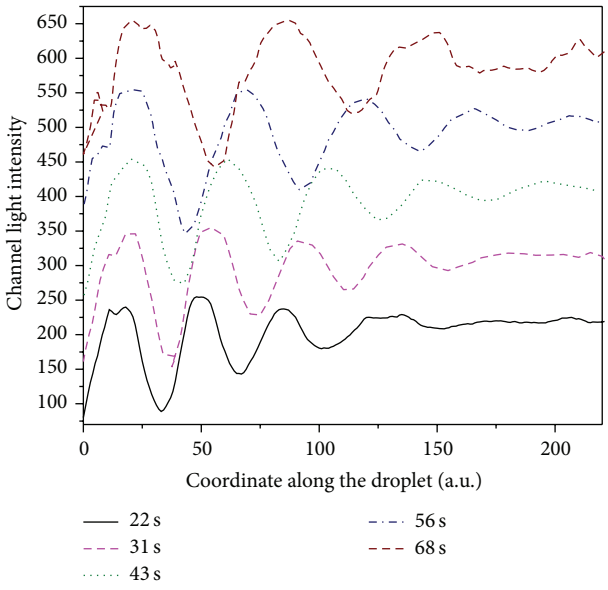

FIGURE 6: Changes in interference pattern corresponding to red channel after injection of VOC that occurred at ca. 20th s (or 10 s after point marked as "Start" in Figure 1).

VOCs in the nematic hosts and data available in the literature suffer from some discrepancies. Also, there are no literature data on maximum VOC concentration in LC matrix. We are currently designing experiments for measuring these parameters; then it would be possible to solve the diffusion equation using the same mesh inside the droplet as before and then directly compare the results of our model calculations with experimental data on kinetics of interference pattern widening. These measurements and calculations lie out of the scope of the present paper. However, it is important to underscore the fact that the widening of interference pattern discovered in this paper can be explained in the framework of the model presented above and clearly indicates the possibility of detecting small concentrations of VOCs. The first detectable shift of interference minima happens in ca. 10 s after injection of VOCs and, therefore, corresponds to a rising part of the curve shown in Figure 1 (this part of the graph is marked as "Inter"). Careful analysis of data for the most sensitive nematic matrix (MBBA) and different VOCs shows that this shift is actually detectable at 3–6 times lower concentrations than those corresponding to saturation. The lowest detectable limits for acetone and toluene were determined to be less than 60 μL/L that is well below corresponding exposure limits of 474 μL/L and 420 μL/L established by US government.

One of the objectives of this work is also to demonstrate that the use of chiral or twisted nematic LCs for gas detection is not limited to cholesteric materials with the selective reflection band lying in a visible range. The changes in fingerprint pattern may also serve as a tool in determination of VOC concentrations in the air. Moreover, for some applications this may be more advantageous than using nematic droplets, the size and shape of which may be difficult to control. The other advantage of using chiral liquid crystals is more freedom in fine tuning the chemical structure of chiral dopants than the chemical structure of liquid crystals, and therefore the relative ease of increasing their sensitivity and selectivity to certain types of VOCs. In a present work the chiral liquid crystals with the helical pitch lying outside of visible range were used. Helical twist was induced in nematic LCs (MBBA, pentylcyanobiphenyl) by chiral dopants available commercially and synthesized in the lab.

Here we present the results for chiral nematic mixture based on MBBA and ethylbenzylamine. The concentration of chiral dopant did not exceed 0.8% that typically produced chiral films with helical pitch in the range of tens of microns. Chiral LCs were spread over the glass surface treated in dodecyl sulfate in order to observe a distinct fingerprint structure of chiral films through the microscope. As in case of the nematic film, the higher concentration of ethanol resulted in isotropisation transition. However, well before the transition to isotropic state two processes occurred. First, the brightness and the contrast of the fingerprint structure changed (although the shape and the details of fingerprint structure remained the same). Second, the fingerprint structure became more "fluid" with changes in the pattern and the period intensified before the transition to isotropic state (Figure 7). The diminishing contrast of fingerprint structure long before the isotropisation transition can be explained in terms of the CLC order parameter decrease in the areas that were affected by a diffusion of VOC molecules. At this stage no changes in helical pitch are observed and we assume that for this stage and this particular pair of chiral dopant and VOC helical pitch changes do not occur. This is the same molecular mechanism that was responsible for changes in interference pattern in case of nematic LCs: decrease of order parameter of the matrix due to the diffusion of low molar mass molecules. The observed changes can be

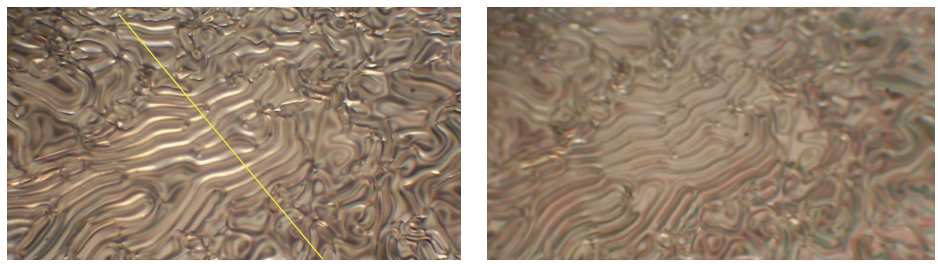

(a) (b)

Figure 7: Visual appearance of fingerprint structure before (a) and after (b) the injection of ethanol.

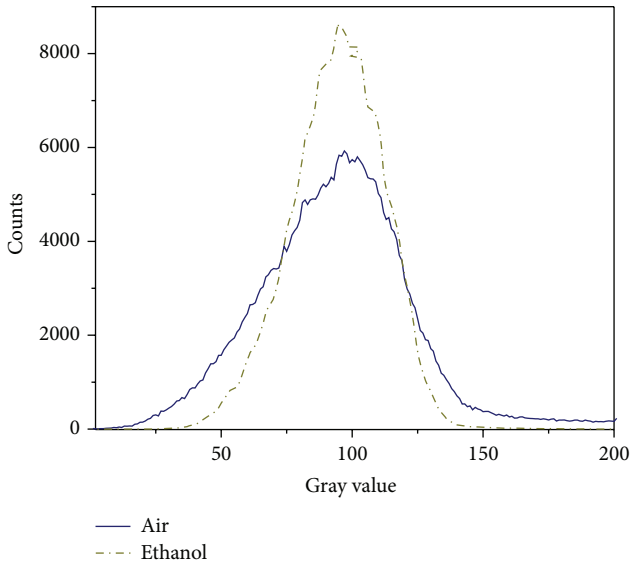

Figure 8: Brightness analysis of the whole chiral fingerprint structure before and after injection of ethanol.

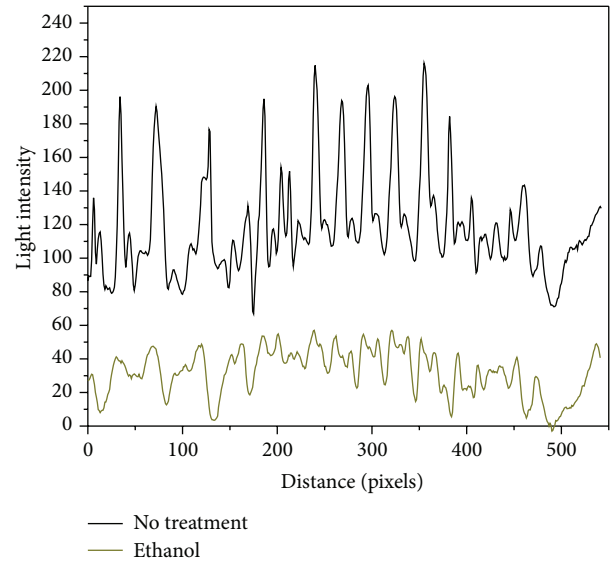

Figure 9: Analysis of light intensity across the fingerprint structure before and after ethanol injection.

analyzed by ImageJ software and quantified by extracting the light intensity distribution (Figure 8) in the photos taken at different VOC concentrations before isotropisation transition. Significant narrowing of dynamic range can be seen in Figure 8 when CLC film is exposed to ethanol vapor. The narrowing is an indicator of VOC presence in the air.

The validity of this analysis is also confirmed by calculations of light intensity changes along the line perpendicular to the fringes (this line is shown as yellow diagonal line in Figure 7). The light intensity is plotted for two different times in Figure 9. The presence of VOC first results in decreasing intensity of peaks and only later, at longer exposures to VOC, it leads to slight changes in their number and positions and, therefore, changes in helical pitch.

Interestingly, these changes occur almost at the same times after injection of ethanol as in case of nematic liquid crystal. In order to check the applicability of the model that takes into account only changes in the order parameter to this particular case of fingerprint structure, we have modeled light propagation through fingerprint structured film. The main features of the model are the same as before: diffusion of VOC results in the formation of a layer with lower order parameter S that in turn leads to changes in the refractive index profile described by (1a) and (1b). The molecular orientation in fingerprint structure is schematically shown in Figure 10: elongated ellipsoids represent projections of molecules on the substrate. Increasing order parameter results in the diminishing eccentricity of each ellipsoid and, therefore, in lowering optical anisotropy. The same methods as in case of nematic LCs were used for calculating light intensity of light transmitted through fingerprint structure. The results of a typical calculation are shown in Figure 11: lower order parameter ($S = 0.52$) leads to apparent decrease in modulation amplitude of light transmitted through the structure. Higher order parameter ($S = 0.7$) results in deeper modulation (the effect depends on a thickness of the layer with lower refractive index and an orientation of fingerprint structure with respect to polarizers).

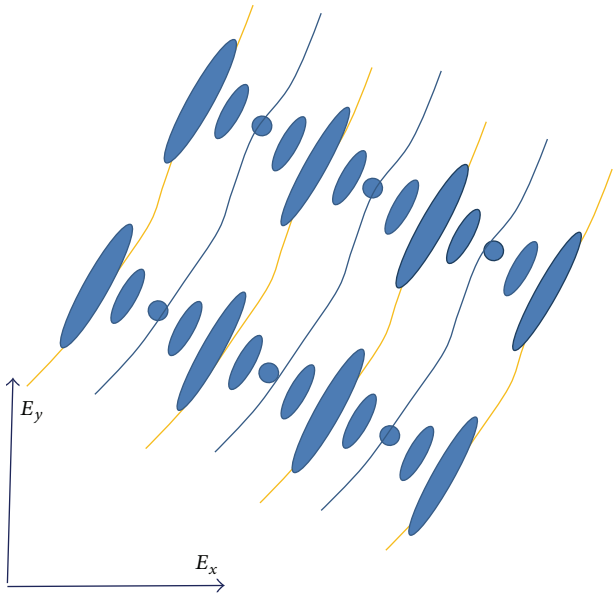

Figure 10: Idealized fingerprint structure, view from the top (compared to the central part of Figure 7). Elongated cylinders represent predominant molecular orientation. E_x and E_y are directions of polarization of incoming and outcoming light. Bright yellow lines correspond to brighter areas in fingerprint structure; dark blue lines correspond to darker areas with homeotropic molecular orientation.

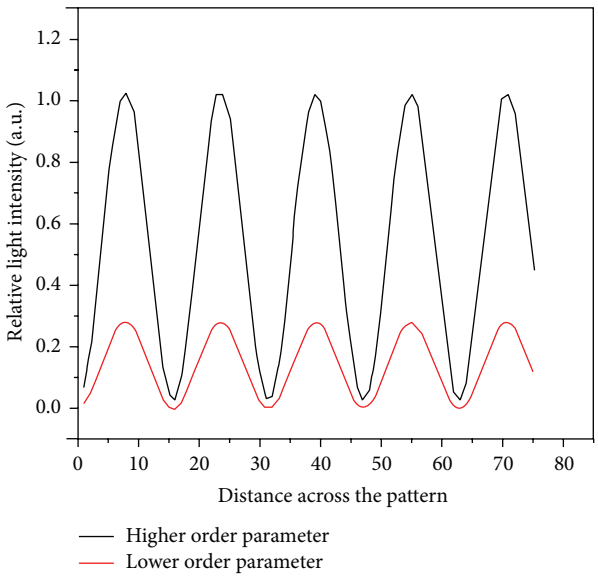

Figure 11: Decrease of light intensity (and contrast) across fingerprint structure at decreased order parameter S.

4. Conclusions

Nematic and cholesteric liquid crystals may find promising applications outside the traditional area of displays and indicators, namely, as sensitive environmental sensors.

The novel criteria for detecting the presence of VOCs in the air are suggested: The analysis of the interference patterns in nematic droplets and distribution of intensity in cholesteric films with fingerprint structure allow detecting VOCs at much lower concentration than by following only isotropisation transition. This is a direct consequence of high sensitivity of interference pattern to changes in the order parameter and, therefore, optical anisotropy. The detection limit of VOC molecules based on this principle is shown to be at least three to six times lower than that based on the detection of isotropisation transition. With CCD and CMOS image sensors widely available the detection of VOCs can become a simple procedure if the image sensors are combined with liquid crystalline sensors. The analysis of photo images can also be easily automated even with the help of modern cell phones.

Conflict of Interests

The authors declare that there is no conflict of interests regarding the publication of this paper.

References

[1] F. Reinitzer, "Beiträge zur Kenntniss des Cholesterins," *Monatshefte für Chemie*, vol. 9, no. 1, pp. 421–441, 1888.

[2] O. Lehmann, "Über fliessende Krystalle," *Zeitschrift für Physikalische Chemie*, vol. 4, p. 462, 1889.

[3] J. A. Castellano, *Liquid Gold: The Story of Liquid Crystal Displays and the Creation of an Industry*, World Scientific, 2005.

[4] P. V. Shibaev, J. Madsen, and A. Z. Genack, "Lasing and narrowing of spontaneous emission from responsive cholesteric films," *Chemistry of Materials*, vol. 16, no. 8, pp. 1397–1399, 2004.

[5] D. S. Miller, R. J. Carlton, P. C. Mushenheim, and N. L. Abbott, "Introduction to optical methods for characterizing liquid crystals at interfaces," *Langmuir*, vol. 29, no. 10, pp. 3154–3169, 2013.

[6] C.-K. Chang, C. M. W. Bastiaansen, D. J. Broer, and H.-L. Kuo, "Alcohol-responsive, hydrogen-bonded, cholesteric liquid-crystal networks," *Advanced Functional Materials*, vol. 22, no. 13, pp. 2855–2859, 2012.

[7] P. V. Shibaev, D. Chiappetta, R. L. Sanford et al., "Color changing cholesteric polymer films sensitive to amino acids," *Macromolecules*, vol. 39, no. 12, pp. 3986–3992, 2006.

[8] M. Khan and S.-Y. Park, "Liquid crystal-based proton sensitive glucose biosensor," *Analytical Chemistry*, vol. 86, no. 3, pp. 1493–1501, 2014.

[9] S. J. Woltman, G. D. Jay, and G. P. Crawford, "Liquid-crystal materials find a new order in biomedical applications," *Nature Materials*, vol. 6, no. 12, pp. 929–938, 2007.

[10] E. J. Poziomek, T. J. Novak, and R. A. Mackay, "Use of liquid crystals as vapor detectors," *Molecular Crystals and Liquid Crystals*, vol. 27, no. 1-2, pp. 175–185, 1974.

[11] J. D. Wright, P. Roisin, G. P. Rigby, R. J. M. Nolte, M. J. Cook, and S. C. Thorpe, "Crowned and liquid-crystalline phthalocyanines as gas-sensor materials," *Sensors and Actuators B: Chemical*, vol. 13, no. 1–3, pp. 276–280, 1993.

[12] N. Kirchner, L. Zedler, T. G. Mayerhöfer, and G. J. Mohr, "Functional liquid crystal films selectively recognize amine vapours and simultaneously change their colour," *Chemical Communications*, no. 14, pp. 1512–1514, 2006.

[13] Y. Han, K. Pacheco, C. W. M. Bastiaansen, D. J. Broer, and R. P. Sijbesma, "Optical monitoring of gases with cholesteric liquid

crystals," *Journal of the American Chemical Society*, vol. 132, no. 9, pp. 2961–2967, 2010.

[14] A. Mujahid, H. Stathopulos, P. A. Lieberzeit, and F. L. Dickert, "Solvent vapour detection with cholesteric liquid crystals—optical and mass-sensitive evaluation of the sensor mechanism," *Sensors*, vol. 10, no. 5, pp. 4887–4897, 2010.

[15] L. Sutarlie, J. Y. Lim, and K.-L. Yang, "Cholesteric liquid crystals doped with dodecylamine for detecting aldehyde vapors," *Analytical Chemistry*, vol. 83, no. 13, pp. 5253–5258, 2011.

[16] X. Ding and K.-L. Yang, "Liquid crystal based optical sensor for detection of vaporous butylamine in air," *Sensors and Actuators B: Chemical*, vol. 173, pp. 607–613, 2012.

[17] C.-K. Chang, H.-L. Kuo, K.-T. Tang, and S.-W. Chiu, "Optical detection of organic vapors using cholesteric liquid crystals," *Applied Physics Letters*, vol. 99, no. 7, Article ID 073504, 2011.

[18] C.-K. Chang, S.-W. Chiu, H.-L. Kuo, and K.-T. Tang, "Cholesteric liquid crystal-carbon nanotube hybrid architectures for gas detection," *Applied Physics Letters*, vol. 100, no. 4, Article ID 043501, 2012.

[19] A. Sen, K. A. Kupcho, B. A. Grinwald, H. J. Vantreeck, and B. R. Acharya, "Liquid crystal-based sensors for selective and quantitative detection of nitrogen dioxide," *Sensors and Actuators, B: Chemical*, vol. 178, pp. 222–227, 2013.

[20] Y.-T. Lai, J.-C. Kuo, and Y.-J. Yang, "A novel gas sensor using polymer-dispersed liquid crystal doped with carbon nanotubes," *Sensors and Actuators A: Physical*, vol. 215, pp. 83–88, 2014.

[21] A. K. Singh, R. Manohar, J. P. Shukla, and A. M. Biradar, "Refractive indices, order parameter and optical transmittance studies of a nematic liquid crystal mixture," *Acta Physica Polonica A*, vol. 110, no. 4, pp. 485–493, 2006.

[22] T. Scharf, *Polarized Light in Liquid Crystals and Polymers*, John Wiley & Sons, 2007.